Excitation spectra and rf response near the polaron-to-molecule transition from the functional renormalization group

Richard Schmidt and Tilman Enss
Physik Department, Technische Universität München, D-85747 Garching, Germany
(Received 11 April 2011; published 15 June 2011)

A light impurity in a Fermi sea undergoes a transition from a polaron to a molecule for increasing interaction. We develop a method to compute the spectral functions of the polaron and molecule in a unified framework based on the functional renormalization group with full self-energy feedback. We discuss the energy spectra and decay widths of the attractive and repulsive polaron branches as well as the molecular bound state, and confirm the scaling of the excited-state decay rate near the transition. The quasiparticle weight of the polaron shifts from the attractive to the repulsive branch across the transition, while the molecular bound state has a very small residue characteristic for a composite particle. We propose an experimental procedure to measure the repulsive branch in a ^{6}Li Fermi gas using rf spectroscopy and calculate the corresponding spectra.

DOI: 10.1103/PhysRevA.83.063620 PACS number(s): 67.85.Lm, 11.10.Gh, 32.30.Bv, 32.70.Jz

I. INTRODUCTION

A single impurity $\downarrow$-atom immersed in a background of $\uparrow$-fermions is a screened Fermi polaron [1] below a critical interaction strength. For larger interaction the ground state changes its character and the impurity forms a molecular bound state with the bath atoms. This qualitative change marks the polaron-to-molecule transition and was predicted by Prokof'ev and Svistunov [2]. The transition can be regarded as the modification of the two-body problem due to medium effects: For two nonrelativistic particles with an interaction characterized by the s-wave scattering length a, a weakly bound molecule is the ground state for positive a, whereas for negative a the molecular state ceases to exist and the ground state is given by the free atoms.

Related impurity models have been studied for many years, in particular the Kondo effect for a fixed impurity with discrete energy levels immersed in a Fermi sea of conduction electrons [3]. A mobile but very heavy impurity loses its quasiparticle character in low dimensions $d = 1$, related to the orthogonality catastrophe [4]. The transition of the light mobile impurity poses a challenging many-body problem.

The polaron-to-molecule transition is observable with ultracold atoms where the scattering length can be tuned via Feshbach resonances [5]. Using radiofrequency (rf) spectroscopy the line shape, ground-state energy, and polaron quasiparticle weight have been measured across the transition [6]. The ground-state properties near the transition have been calculated using variational wave functions [7–13], non-self-consistent T-matrix approximations [8], $1/N$ expansions [14], Wilsonian renormalization group [15], variational Monte Carlo [16], and diagrammatic Monte Carlo (diagMC) [2].

It turns out that even beyond the critical interaction strength the polaron remains as a long-lived excitation above the molecular ground state and, conversely, the molecule becomes an excited state on the polaronic side of the transition. The proper description of these excited states and, in particular, their finite lifetime remains a difficult problem. Using a phenomenological model in a three-loop calculation, Bruun and Massignan have shown that the decay rates of the excited states decrease rapidly as $\Delta\omega^{9/2}$ toward the transition, where $\Delta\omega$ is the energy difference between the ground and excited states [17].

Recently, interest has focused on an additional feature present in the polaron-to-molecule transition: The renormalization of the $\downarrow$-spectral function by the strong interactions leads to the appearance of an additional quasiparticle excitation for positive energies. This excitation corresponds to a Fermi polaron interacting repulsively with the $\uparrow$-Fermi sea. The repulsive polaron has a finite lifetime which becomes very small at unitarity, $a \to \infty$. In the opposite limit of weak coupling $a \to 0$, the repulsive polaron is long-lived and its spectral weight approaches unity. This justifies perturbative methods which neglect the presence of the molecular channel [18,19]. The repulsive polaron has been studied theoretically in the context of ultracold gases by Cui and Zhai [20] and more recently by Massignan and Bruun [21]. Experimentally, the repulsive polaron has not yet been observed in the strong-coupling regime. However, it has important implications for the stability of a ferromagnetic phase in Fermi gases [20,22–26]. Furthermore, a single $\downarrow$-fermion in an $\uparrow$-Fermi sea corresponds to a strongly imbalanced, two-component Fermi gas near full polarization, and the polaron-to-molecule transition sheds light on a region of the zero-temperature phase diagram of the polarized Fermi gas [10,15,27].

So far, there is a lack of theoretical work which describes all of these features within one unified approach. In this paper we present a method capable of doing this. By devising a new numerical implementation of the functional renormalization group (fRG) we are able to determine both the full spectral functions and the quasiparticle features of the polaron-to-molecule transition.

With the renormalization group one usually limits oneself to a few running couplings. In this work we develop a computational tool which allows us to keep track of the renormalization group flow of fully momentum- and frequency-dependent Matsubara Green's functions based on an exact renormalization group equation [28]. By introducing an auxiliary bosonic field which mediates the interaction between $\uparrow$- and $\downarrow$-atoms, we are able to accurately capture the momentum and frequency dependence of both vertex functions and propagators. In particular for nonuniversal quantities,

our approach, which complements the proposal by Blaizot, Méndez-Galain, and Wschebor [29], may prove vital, and we demonstrate its efficiency in the polaron problem.

Our main results from the fRG are the following: We give not only the spectral functions of the $\downarrow$-fermion but also of the molecule in a wide range of interaction values. From this we extract the quasiparticle properties including energies, decay rates, and residues for both the polaron and the molecule. We connect the quasiparticle weight of the molecule with a measure of its compositeness introduced by Weinberg [30]. We propose a new experimental procedure to measure the repulsive polaron in a ^{6}Li Fermi gas using rf spectroscopy, and we employ our spectral functions to predict the expected rf response.

The paper is organized as follows: in Sec. II we introduce the model of the polaron-to-molecule transition and derive appropriate fRG flow equations. These equations are solved in Sec. III for the full frequency- and momentum-dependent spectral functions, which are presented and interpreted in Sec. IV. Section V is devoted to rf spectroscopy, and we conclude with a discussion in Sec. VI. In the appendix the fRG flow equations are solved using the simpler derivative expansion, which already gives qualitatively correct results.

II. MODEL AND RG FLOW EQUATIONS

In this work we study a two-component Fermi gas in the limit of extreme population imbalance at $T = 0$. The microscopic action describing the system is

$$S = \int_{\mathbf{x},\tau} \Big\{ \sum_{\sigma=\uparrow,\downarrow} \psi_\sigma^*[\partial_\tau - \Delta - \mu_\sigma]\psi_\sigma + g\psi_\uparrow^*\psi_\downarrow^*\psi_\downarrow\psi_\uparrow \Big\}, \tag{1}$$

in natural units $\hbar = 2m = 1$ and with imaginary time τ. The Grassmann-valued, fermionic fields $\psi_\uparrow$ and $\psi_\downarrow$ denote the up and down fermions, respectively, which have equal mass m. The associated chemical potentials μ_σ are adjusted such that the $\uparrow$-fermions have a finite density $n_\uparrow = k_F^3/(6\pi^2)$ while there is only a single impurity $\downarrow$-fermion. The atoms interact via a contact interaction with coupling constant g which is related to the s-wave scattering length a via $g = 8\pi a$. The T-matrix acquires a complicated frequency and momentum dependence in the strong-coupling limit. It is then convenient to perform a Hubbard-Stratonovich transformation of the action (1) by introducing a bosonic molecule (pairing) field $\phi \sim \psi_\downarrow\psi_\uparrow$ which mediates the two-particle interaction $g\psi_\uparrow^*\psi_\downarrow^*\psi_\downarrow\psi_\uparrow$. The resulting action is given by

$$S = \int_{\mathbf{x},\tau} \Big\{ \sum_{\sigma=\uparrow,\downarrow} \psi_\sigma^*[\partial_\tau - \Delta - \mu_\sigma]\psi_\sigma + \phi^* G_{\phi,\Lambda}^{-1}\phi + h(\psi_\uparrow^*\psi_\downarrow^*\phi + \text{H.c.}) \Big\}, \tag{2}$$

with a real Yukawa coupling h for the conversion of two fermions into a molecule. Integrating out the bosonic field ϕ shows that (2) is equivalent to the single-channel model (1) provided that $-h^2 G_{\phi,\Lambda} = g$ and $h \to \infty$ [14,31]. As $h^2 \sim \Delta B$ this limit corresponds to a broad Feshbach resonance [5].

The physical properties can be accessed via Green's functions which are derivable from generating functionals. The one-particle irreducible vertex functions $\Gamma^{(n)}$ are obtained from the effective quantum action Γ, which can, for instance, be computed perturbatively in a loop expansion. As we are interested in the intrinsically nonperturbative regime of fermions close to a Feshbach resonance where the scattering length a diverges, we employ a different approach. Γ includes quantum fluctuations on all momentum and energy scales. The main idea of the functional renormalization group (fRG) is to introduce an interpolating effective flowing action Γ_k which includes only fluctuations on momentum scales $q \gtrsim k$ larger than the renormalization group scale k. At the UV scale $k = \Lambda \to \infty$ the effective flowing action reduces to the microscopic action S which does not include any quantum corrections. In the infrared limit $k \to 0$, Γ_k equals the full quantum action Γ.

The evolution, or flow, of Γ_k with the RG scale k is given by the exact renormalization group equation [28]

$$\partial_k \Gamma_k = \frac{1}{2}\,\mathrm{STr}\left(\frac{1}{\Gamma_k^{(2)} + R_k}\partial_k R_k\right). \tag{3}$$

The supertrace symbol STr denotes a loop integration over frequency and momentum as well as the summation over all fields and internal degrees of freedom, with a minus sign for fermions. $\Gamma_k^{(2)}$ is the full, field-dependent inverse two-point Green's function at scale k, and R_k is a regulator taking care of the successive inclusion of momentum scales. The regulator acts by imposing a large mass term on the modes with momenta $q \lesssim k$ lower than the cutoff scale k. R_k can be chosen freely as long as $R_{k\to 0} \to 0$ and $R_{k\to\infty} \to \infty$. For further details on the fRG we refer to the literature [32–34], and to its application to the Bose-Einstein-condensate– (BEC–) BCS crossover [35].

Γ_k is in general a functional of the fields and contains all possible operators of the fields allowed by the symmetries. For this reason its exact calculation is usually impossible and one has to rely on approximations for Γ_k. In this work we will use the truncation

$$\Gamma_k = \int_{\mathbf{p},\omega} \big\{ \psi_\uparrow^*[-i\omega + \mathbf{p}^2 - \mu_\uparrow]\psi_\uparrow + \psi_\downarrow^* G_{\downarrow,k}^{-1}(\omega,\mathbf{p})\psi_\downarrow + \phi^* G_{\phi,k}^{-1}(\omega,\mathbf{p})\phi \big\} + \int_{\mathbf{x},\tau} h(\psi_\uparrow^*\psi_\downarrow^*\phi + \text{H.c.}), \tag{4}$$

with Matsubara frequency ω. For the momentum and frequency dependence of the k-dependent, or flowing, propagators of the $\downarrow$-fermion $G_{\downarrow,k}$ and the boson $G_{\phi,k}$ we will present a simple approximation in terms of a gradient expansion in the appendix. In the following Sec. III we develop a new numerical method to solve the renormalization group flow of the propagators as completely general functions of ω and $\mathbf{p}$. This will enable us to capture decay rates and dynamic effects which is not possible in a simple gradient expansion.

Within the truncation (4), the Yukawa coupling h is not renormalized, which can be seen by a simple argument. In Eq. (4) we neglect a term $\psi_\uparrow^*\psi_\downarrow^*\psi_\downarrow\psi_\uparrow$ which would be regenerated during the flow by particle-hole fluctuations [36]. Similarly, a term $\psi_\uparrow^*\phi^*\psi_\uparrow\phi$ for the atom-dimer interaction is neglected. Both terms would lead to a renormalization of h. Due to their omission, however, there is no diagram generating

a flow of h which is why $\partial_k h \equiv 0$ and h remains independent of frequency and momentum. Furthermore, we neglect terms $(\phi^*\phi)^{n\geq 2}$ which would give higher-order corrections to the bosonic self-energy. The majority $\uparrow$-atoms are renormalized only by the single impurity $\downarrow$-atom to order $1/N_\uparrow$, hence one can neglect the renormalization of the $\uparrow$-atoms in the thermodynamic limit, and the chemical potential $\mu_\uparrow = \epsilon_F = k_F^2/(2m)$ is that of a free Fermi gas (we work in units where the Fermi momentum $k_F = 1$) [2].

As Eq. (3) is a (functional) differential equation, it has to be supplemented with appropriate initial conditions at the UV scale Λ, which are obtained from few-body (vacuum) physics. The s-wave vacuum scattering amplitude for the interaction of an $\uparrow$- and $\downarrow$-fermion with momenta $\mathbf{q}, -\mathbf{q}$ in the center-of-mass frame is given by ($q = |\mathbf{q}|$)

$$f(q) = \frac{1}{-1/a - iq}. \tag{5}$$

$f(q)$ is related to the full molecule propagator $G^{\text{vac}}_{\phi,\text{R}}$ evaluated at the infrared RG scale $k = 0$,

$$f(q) = \frac{h^2}{8\pi} G^{\text{vac}}_{\phi,\text{R}}(\omega = 2q^2, \mathbf{p} = 0), \tag{6}$$

where $\omega = 2q^2$ is the total kinetic energy of the interacting atoms. The subscript R indicates that the analytical continuation to the retarded function of real frequencies ($i\omega \to \omega + i0$) has been performed. In Ref. [37] the exact vacuum molecule propagator $G^{\text{vac}}_{\phi,\text{R}}$ has been calculated using the fRG and agrees with the well-known result

$$\left[G^{\text{vac}}_{\phi,\text{R}}(\omega,\mathbf{p})\right]^{-1} = \frac{h^2}{8\pi}\left(-a^{-1} + \sqrt{-\frac{\omega}{2} + \frac{\mathbf{p}^2}{4} - i0}\right). \tag{7}$$

This expression for $G^{\text{vac}}_{\phi,\text{R}}$ reproduces the correct scattering amplitude (5) when inserted into Eq. (6), and dictates the form of the UV propagator $G^{-1}_{\phi,\Lambda}$ for a given choice of regulator.

Furthermore, the initial condition for the fermions is given by their form in the microscopic action (2), $G^{-1}_{\sigma,k=\Lambda}(\omega,\mathbf{p}) = -i\omega + \mathbf{p}^2 - \mu_\sigma$. As we will see in the following, the momentum and frequency dependence of both propagators, $G_{\phi,k}$ and $G_{\downarrow,k}$, is strongly renormalized during the fRG flow toward the infrared, which leads to a rich structure of the spectral functions.

After inserting the truncation (4) into the flow equation (3), the flow of $G_{\downarrow,k}$ and $G_{\phi,k}$ is derived by taking the appropriate functional derivatives of Eq. (3) with respect to the fields. One obtains the fRG flow equations

$$\begin{aligned}
\partial_k P_{\downarrow,k}(P) &= h^2 \tilde{\partial}_k \int_Q G^c_{\phi,k}(Q) G^c_{\uparrow,k}(Q - P), \\
\partial_k P_{\phi,k}(P) &= -h^2 \tilde{\partial}_k \int_Q G^c_{\downarrow,k}(Q) G^c_{\uparrow,k}(P - Q),
\end{aligned} \tag{8}$$

with the multi-indices $P = (\omega,\mathbf{p})$ and $Q = (\nu,\mathbf{q})$. The $P_k \equiv G_k^{-1}$ on the left-hand side are the flowing inverse propagators without the regulator from Eq. (4), while the propagators G^c_k on the right-hand side are regulated:

$$G_k \equiv 1/P_k, \quad G^c_k \equiv 1/(P_k + R_k). \tag{9}$$

The tilde on $\tilde{\partial}_k$ indicates that the derivative with respect to the RG scale k acts only on the regulator term R_k in the cutoff propagators G^c_k. Specifically, the single-scale propagators read $\tilde{\partial}_k G^c_k = -(G^c_k)^2 \partial_k R_k$ in Eq. (8). Note that the flow equations (8), which are depicted in Fig. 1, have a one-loop structure but contain the full propagators at scale k. By integrating the flow, diagrams of arbitrarily high loop order are generated and constantly fed back into each other. It is especially for the latter reason that our approach goes beyond other approximations used for the description of the polaron problem, such as, for example, the non-self-consistent T-matrix approximation [8,21]. The goal of this paper is to solve the system of differential flow equations (8).

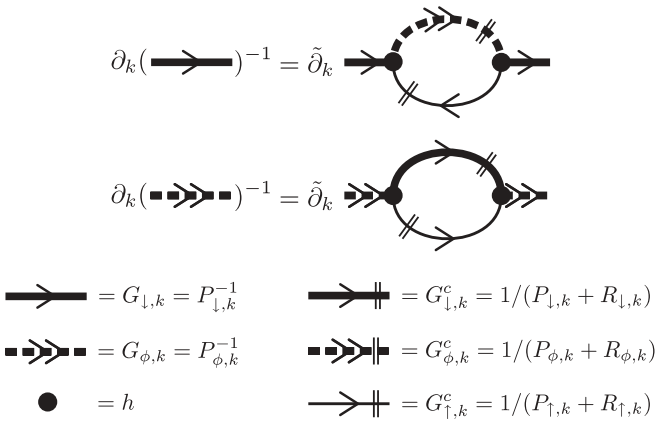

FIG. 1. Diagrammatic representation of the fRG flow equations (8) for the impurity and molecule propagators.

In the following we choose sharp cutoff functions R_k which strictly cut off all momentum modes with $|\mathbf{p}| < k$ while the frequencies are not restricted.[1] Then the regulated Green's functions G^c_k take the particularly simple form (for unoccupied $\downarrow$-atoms)

$$\begin{aligned}
G^c_{\downarrow,k}(\omega,\mathbf{p}) &= \frac{\theta(|\mathbf{p}| - k)}{P_{\downarrow,k}(\omega,\mathbf{p})}, \\
G^c_{\phi,k}(\omega,\mathbf{p}) &= \frac{\theta(|\mathbf{p}| - k)}{P_{\phi,k}(\omega,\mathbf{p})}, \\
G^c_{\uparrow,k}(\omega,\mathbf{p}) &= \frac{\theta(|\mathbf{p}^2 - \mu_\uparrow| - k^2)}{P_{\uparrow,k}(\omega,\mathbf{p})}.
\end{aligned} \tag{10}$$

For the $\uparrow$-atoms it is crucial to regularize the low-energy modes around the Fermi energy $\mu_\uparrow$. Using the Dyson equation

$$P_k(\omega,\mathbf{p}) = G_k^{-1}(\omega,\mathbf{p}) = G_0^{-1}(\omega,\mathbf{p}) - \Sigma_k(\omega,\mathbf{p}),$$

where $G_0 = G_{k=\Lambda}$ denotes the free (UV) and G_k the full Green's function at scale k, we can in particular identify the gap term

$$m^2_{\downarrow,k} := P_{\downarrow,k}(0,\mathbf{0}) = -\mu_\downarrow - \Sigma_{\downarrow,k}(0,\mathbf{0}). \tag{11}$$

[1]While the solution of the untruncated flow equation (3) does not depend on the particular choice of the cutoff function, the results from the truncated flow become cutoff-dependent. We implemented a class of smooth cutoff functions interpolating between a k^2 and the sharp cutoff and found minimal sensitivity [34,38] and also the best agreement with Monte Carlo data for the limit of the sharp cutoff.

TABLE I. Conditions for the polaron and molecule ground states.

Coupling	$(k_F a)^{-1} < (k_F a_c)^{-1}$	$(k_F a)^{-1} > (k_F a_c)^{-1}$
Ground State	Polaron	Molecule
$\downarrow$ gap	$P_\downarrow(0,\mathbf{0}) = m_\downarrow^2 = 0$	$P_\downarrow(0,\mathbf{0}) = m_\downarrow^2 > 0$
ϕ gap	$P_\phi(0,\mathbf{0}) = m_\phi^2 > 0$	$P_\phi(0,\mathbf{0}) = m_\phi^2 = 0$

The chemical potential $\mu_\downarrow$ is the energy required to add one $\downarrow$-atom to the system,

$$\mu_\downarrow = E(N_\downarrow) - E(N_\downarrow - 1), \tag{12}$$

and is independent of the cutoff scale k. The interaction effects on the $\downarrow$-fermion, which are successively included during the flow, are captured by the k-dependent self-energy $\Sigma_k(\omega,\mathbf{p})$. In the polaron problem we are interested in a two-component Fermi gas in the limit of extreme population imbalance where one considers only a single $\downarrow$-atom, $N_\downarrow = 1$, and relation (12) is used to determine the ground-state energy of the system. This value of the chemical potential $\mu_\downarrow$ then marks the phase transition from a degenerate, fully polarized $\uparrow$-Fermi gas to a phase of finite $\downarrow$-fermion density [10]. Accordingly, for all choices of $\mu'_\downarrow \leqslant \mu_\downarrow$ there has to be a vanishing occupation of both $\downarrow$-fermions and molecules at every RG scale k, which leads to the condition

$$P_{\downarrow,k}(0,\mathbf{0},\mu'_\downarrow) \geqslant 0, \quad P_{\phi,k}(0,\mathbf{0},\mu'_\downarrow) \geqslant 0 \quad \forall\, \mu'_\downarrow \leqslant \mu_\downarrow. \tag{13}$$

In order to have only a single $\downarrow$-atom or molecule, $\mu_\downarrow$ has to be determined self-consistently such either the $\downarrow$-atom or the molecule ϕ is gapless in the infrared, $P_{\downarrow/\phi,k=0}(0,\mathbf{0}) = 0$ (ground state). We find that, depending on the value of the dimensionless coupling $(k_F a)^{-1}$, either the polaron or the molecule becomes the ground state, see Table I. The polaron-to-molecule transition occurs at the critical interaction strength $(k_F a_c)^{-1}$ at which $m_\phi^2 = m_\downarrow^2 = 0$.

III. RG FOR FULL SPECTRAL FUNCTIONS

The main goal of this work is to solve the system of flow equations (8) without imposing any constraints on the frequency and momentum dependence of the polaron and molecule propagators. This problem can only be solved numerically, and the inverse, flowing Green's functions $P_{\downarrow/\phi,k}(\omega,\mathbf{p})$ are evaluated on a discrete grid in frequency and momentum space,

$$\begin{aligned} P_{\downarrow,k}(\omega,\mathbf{p}) &\to P_{\downarrow,k}(\omega_i,p_j) = P^{ij}_{\downarrow,k}, \\ P_{\phi,k}(\omega,\mathbf{p}) &\to P_{\phi,k}(\omega_i,p_j) = P^{ij}_{\phi,k}. \end{aligned} \tag{14}$$

We choose a logarithmically spaced, finite grid with $\omega_i \in (0,\ldots,\omega_{\max})$ and $p_j \in (0,\ldots,p_{\max})$. As a result of rotational invariance, the propagators depend only on the magnitude of spatial momentum $p = |\mathbf{p}|$ and, due to the condition $P^*(\omega) = P(-\omega)$ for Euclidean (Matsubara) propagators, it is sufficient to consider positive frequencies only [39]. The full (ω,p) dependence is reconstructed from the finite number of couplings $P^{ij}_{\downarrow/\phi,k}$ by cubic spline interpolation,

$$\begin{aligned} P_{\downarrow/\phi,k}(\omega,p) &= \mathrm{Spline}\big(\{P^{ij}_{\downarrow/\phi,k}\}\big) \\ &= \sum_{\xi,\vartheta=0}^{3} c^{ij,\xi\vartheta}_{\downarrow/\phi,k}(\omega-\omega_i)^\xi (p-p_j)^\vartheta, \end{aligned} \tag{15}$$

with $\omega \in (\omega_i,\omega_{i+1})$, $p \in (p_j,p_{j+1})$, and where $c^{ij,\xi\vartheta}_{\downarrow/\phi,k}$ are the corresponding spline coefficients. For the asymptotics of the propagators for high frequency and momentum modes, $\omega > \omega_{\max}$ and/or $p > p_{\max}$, we choose the simple fit models

$$\begin{aligned} P^{>}_{\downarrow,k}(\omega,\mathbf{p}) &= -i\omega + \mathbf{p}^2 - \mu_\downarrow, \\ P^{>}_{\phi,k}(\omega,\mathbf{p}) &= \frac{h^2}{8\pi}\left(-a^{-1} + \sqrt{-\frac{i\omega}{2} + \frac{\mathbf{p}^2}{4} + f_{\phi,k}}\right), \end{aligned} \tag{16}$$

with $f_{\phi,k}$ determined by a continuity condition from the numerical value of $P_{\phi,k}$ for the largest momenta $|\mathbf{p}| = p_{\max}$.

In order to keep the numerical cost of computing the flow equations (8) low, it is advantageous to employ the sharp momentum regulator functions $R_{\downarrow,k}$, $R_{\uparrow,k}$, and $R_{\phi,k}$ defined by Eq. (10). This reduces the number of loop integrations by one. The flow equations evaluated by our algorithm are then given by

$$\begin{aligned} \partial_k P_{\downarrow,k}(\omega,\mathbf{p}) &= -\frac{h^2}{(2\pi)^3}\int_{-1}^{1} dx \int_{-\infty}^{\infty} d\nu \int_0^\infty q^2 dq \\ &\quad \times \frac{\chi_k^-(p,q,x)}{P_{\phi,k}(\nu,\mathbf{q}) P_{\uparrow,k}(\nu-\omega,\vec{q}-\vec{p})}, \\ \partial_k P_{\phi,k}(\omega,\mathbf{p}) &= \frac{h^2}{(2\pi)^3}\int_{-1}^{1} dx \int_{-\infty}^{\infty} d\nu \int_0^\infty q^2 dq \\ &\quad \times \frac{\chi_k^-(p,q,x)}{P_{\downarrow,k}(\nu,\mathbf{q}) P_{\uparrow,k}(\omega-\nu,\mathbf{p}-\mathbf{q})}, \end{aligned} \tag{17}$$

where we have defined the characteristic functions

$$\begin{aligned} \chi_k^\pm(p,q,x) &= \delta(q-k)\theta(|(\mathbf{p}\pm\mathbf{q})^2 - \mu_\uparrow| - k^2) \\ &\quad + 2k\theta(q-k)\delta(|(\mathbf{p}\pm\mathbf{q})^2 - \mu_\uparrow| - k^2), \end{aligned} \tag{18}$$

and $x = \cos\theta$ expresses the angle θ between the momentum vectors $\mathbf{p}$ and $\mathbf{q}$ such that $|\mathbf{p}\pm\mathbf{q}|^2 = p^2 + q^2 \pm 2pqx$.

The initial condition at the UV scale $k = \Lambda$ is determined by the few-body calculation (7). As we employ no approximation for the momentum and frequency dependence of the molecule propagator we are able to incorporate the exact two-body scattering amplitude (5), in contrast to the calculation in the appendix using the derivative expansion where this is not possible. The vacuum problem can be solved exactly using the sharp regulators (10), which leads to the UV molecule propagator

$$\begin{aligned} P_{\phi,\Lambda}(\omega,\mathbf{p}) &= -\frac{h^2}{8\pi a} + \frac{h^2\Lambda}{4\pi^2} - \frac{h^2}{2} \\ &\quad \times \int_{\mathbf{q}}\left[\frac{\theta\big(|\mathbf{q}-\frac{\mathbf{p}}{2}|-\Lambda\big)\theta\big(|\mathbf{q}+\frac{\mathbf{p}}{2}|-\Lambda\big)}{q^2 + \big(-\frac{i\omega}{2} + \frac{\mathbf{p}^2}{4} - \mu_{\mathrm{vac}}\big)} - \frac{\theta(q-\Lambda)}{q^2}\right]. \end{aligned}$$

At each RG step we first perform the q integration in Eq. (17) which is trivial due to the δ functions in the characteristic functions $\chi_k^{\pm}$. Next the frequency integration in Eq. (17) is carried out. The computational speed is greatly enhanced by mapping the numerical integration onto an analytical integration using the spline polynomials in the interval $(-\omega_{\max},\omega_{\max})$. $\omega_{\max}$ is chosen such that the error in the ω integration of the outer regime $\omega > \omega_{\max}$ introduced due to the approximation (16) is smaller than the accuracy of the numerical solution of the system of differential equations (8). For the final angular integration in $x = \cos\theta$ on the right-hand side of the flow equation (17) we use a numerical integration with adaptive nodes in order to cope with discontinuities of the integrand.

In order to obtain a stable numerical result it is sufficient to calculate the flow of the propagators for roughly 1500 grid points (ω_i, p_j) in frequency and momentum space. The corresponding system of ordinary differential equations is straightforwardly solved using a Runge-Kutta algorithm, which we have implemented in a version with adaptive stepsize in RG time $t = \ln(k/\Lambda)$. An adaptive stepsize is essential in order to detect the kinks in the RG flow due to the sharp Fermi surface of the $\uparrow$-fermions at zero temperature. We observe that about 10^4 RG steps are necessary to obtain an error smaller than $\epsilon \sim 10^{-5}$.

Finally, when the flow reaches the infrared, $k = 0$, we end up with the full Matsubara Green's functions $G_{\downarrow,k=0}(\omega,p)$ and $G_{\phi,k=0}(\omega,p)$. The initial value of $\mu_\downarrow$ for a given $k_F a$ is adjusted such that a vanishing macroscopic occupation of $\downarrow$-atoms and molecules is obtained at the end of the flow, as discussed in Sec. II. In order to access the spectral functions we perform the analytical continuation to real frequencies by using a Padé approximation.

IV. FULL SPECTRAL FUNCTIONS

We now present our numerical results for the spectral functions of the polaron and molecule across the whole transition region. First, the Matsubara Green's functions at the end of the RG flow, $G_{\downarrow/\phi,k=0}(\omega,\mathbf{p})$, are continued analytically to retarded Green's functions of real frequency, $G_{\downarrow/\phi,\mathrm{R}}(\omega,\mathbf{p})$, using the Padé approximation. The spectral functions are defined as

$$A_{\downarrow/\phi}(\omega,\mathbf{p}) = 2\,\mathrm{Im}\,G_{\downarrow/\phi,\mathrm{R}}(\omega,\mathbf{p}). \tag{19}$$

In Fig. 2 the zero-momentum spectral functions $A_{\downarrow/\phi}(\omega,\mathbf{p} = 0)$ are shown as functions of frequency and coupling $(k_F a)^{-1}$.

The coherent single-particle excitations at zero momentum are determined by the solutions ω_{qp} of the equation

$$G^{-1}_{\downarrow/\phi,\mathrm{R}}(\omega,\mathbf{p} = 0)|_{\omega=\omega_{\mathrm{qp}}} = 0 \tag{20}$$

for ω in the complex lower half-plane. Near each quasiparticle pole the retarded propagator can be approximated by the form

$$G_{\downarrow/\phi,\mathrm{R}}(\omega,\mathbf{p} = 0) \approx \frac{Z_{\downarrow/\phi}}{\omega_{\mathrm{qp}} - \omega - i0}, \tag{21}$$

where the real part of ω_{qp} determines the quasiparticle energy

$$E_{\mathrm{qp}} = \mu_\downarrow + \mathrm{Re}[\omega_{\mathrm{qp}}]. \tag{22}$$

We have shifted the ground-state energy, which is zero in our calculation (vanishing gap), to the conventional value $\mu_\downarrow$ from Eq. (12). The imaginary part of the pole position determines the decay width

$$\Gamma_{\mathrm{qp}} = -\,\mathrm{Im}[\omega_{\mathrm{qp}}]. \tag{23}$$

A Fourier transform in time relates the decay width to the quasiparticle lifetime

$$\tau_{\mathrm{qp}} = \hbar/\,\Gamma_{\mathrm{qp}}. \tag{24}$$

The quasiparticle weight $Z_{\downarrow/\phi}$ is obtained from the frequency slope at the complex pole position,

$$Z^{-1}_{\downarrow/\phi} = -\frac{\partial}{\partial\omega} G^{-1}_{\downarrow/\phi,\mathrm{R}}(\omega,\mathbf{p} = 0)|_{\omega=\omega_{\mathrm{qp}}}. \tag{25}$$

Note that an alternative definition of the decay width in terms of the self-energy evaluated not at the complex pole position but on the real frequency axis,

$$\Gamma_{\mathrm{alt}} = \mathrm{Im}\,\Sigma_{\downarrow/\phi,\mathrm{R}}(\omega,\mathbf{p} = 0)|_{\omega=\mathrm{Re}\,\omega_{\mathrm{qp}}}, \tag{26}$$

agrees with our definition for Γ_{qp} only for a single quasiparticle pole (21) with $Z = 1$. However, for the polaron problem there are further excited states and $Z < 1$. Hence, only Γ_{qp} from Eq. (23) can be interpreted as the halfwidth of the peaks in the spectral function and as the inverse lifetime.

We will now in turn discuss the features seen in the spectral functions—the peak position E_{qp}, width Γ_{qp}, and weight Z—first for the polaron (upper row of Fig. 2) and then for the molecule (lower row).

A. Attractive and repulsive polaron

Energy spectrum. Let us first look at the energy spectrum of the quasiparticle excitations depicted in Fig. 3 in dependence on the coupling strength $(k_F a)^{-1}$. From our data we find two coherent quasiparticle states for the $\downarrow$-atom, the attractive and the repulsive polaron, and one bound state for the molecule. The attractive polaron (red solid line) is the ground state for $(k_F a)^{-1} < (k_F a_c)^{-1}$ (polaronic side) but becomes an excited state for $(k_F a)^{-1} > (k_F a_c)^{-1}$ (molecular side). Conversely, the molecule is the ground state on the molecular side (blue dashed line) and an excited state on the polaronic side, in accordance with the discussion at the end of Sec. II. For the critical coupling strength we obtain $(k_F a_c)^{-1} = 0.904(5)$, which agrees with the value $(k_F a_c)^{-1} = 0.90(2)$ obtained using diagrammatic Monte Carlo (diagMC) by Prokof'ev and Svistunov [2]. As shown in the inset of Fig. 3, also the values for the energies agree well with diagMC (symbols). At unitarity, $(k_F a)^{-1} = 0$, we obtain the ground-state energy $\mu_\downarrow = -0.57\epsilon_F$ while diagMC gives the value $\mu_\downarrow = -0.615\epsilon_F$. Having treated the full frequency and momentum dependence of the propagators in the truncation (4), we can attribute the residual deviation in the ground-state energy to the omission of the terms $\psi^*_\uparrow\psi^*_\downarrow\psi_\downarrow\psi_\uparrow$ and $\phi^*\psi^*_\sigma\phi\psi_\sigma$. The latter term describes the atom-dimer interaction and is expected to further reduce the ground-state energy in the transition regime in accordance with the results from the variational wave-function approach [10,11]. The term $\psi^*_\uparrow\psi^*_\downarrow\psi_\downarrow\psi_\uparrow$, generated by particle-hole fluctuations, is expected to give the main correction in the unitarity regime [9]. Both terms can be included in the fRG

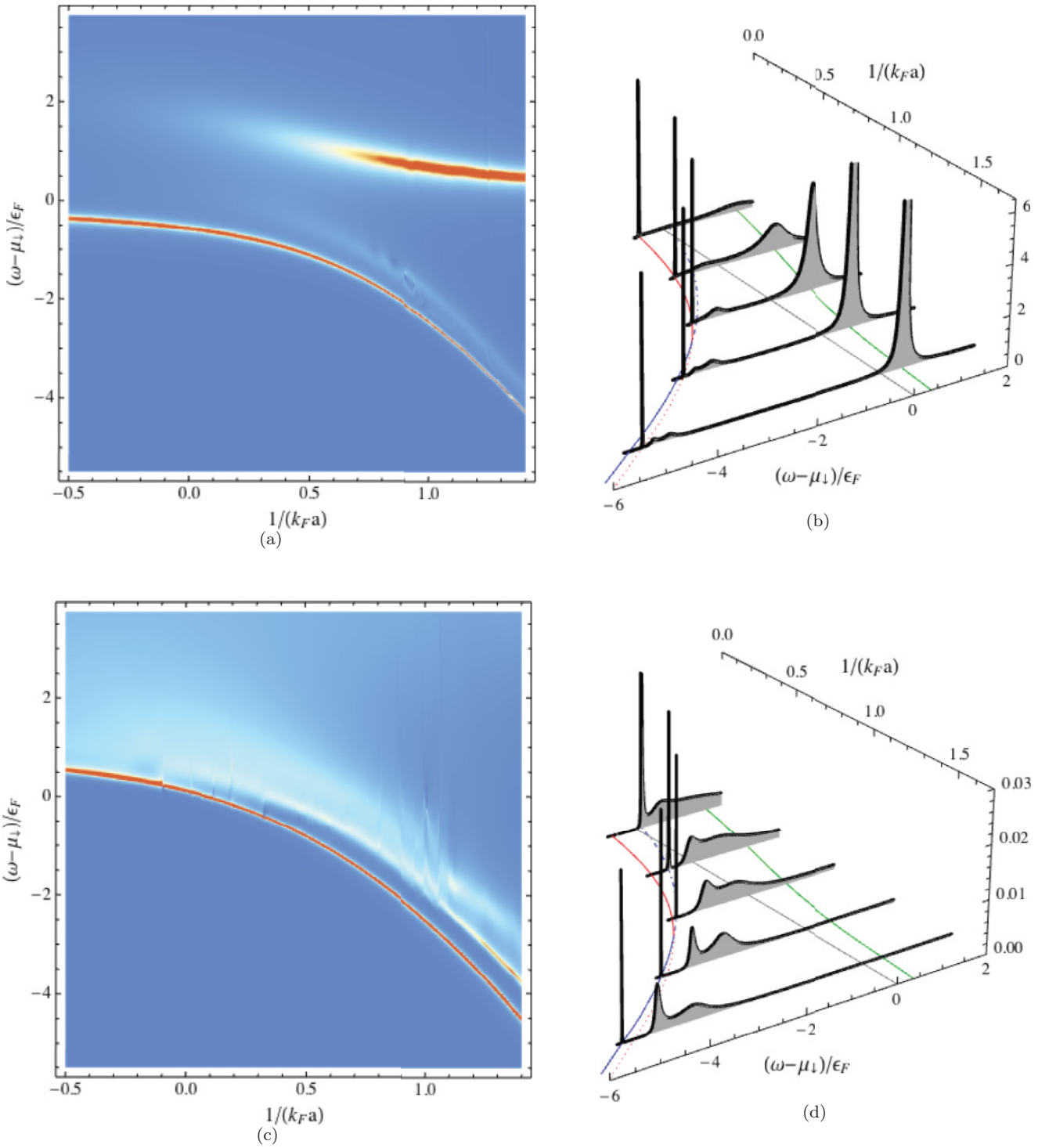

FIG. 2. (Color online) Spectral functions at zero momentum in dependence on $1/(k_F a)$. (a), (b) Polaron spectral function $A_\downarrow(\omega, \mathbf{p} = 0)$. (c), (d) Molecule spectral functions $A_\phi(\omega, \mathbf{p} = 0)$. In order to make the δ-function peak for the ground state visible we introduced an artificial width of the quasiparticles of $0.007\epsilon_F$.

flow as additional flowing couplings, or implicitly by using the Katanin scheme [40] or rebosonization [41].

Until recently [22] most experiments with ultracold Fermi gases have focused on the lower, attractive branch on the BEC side $(k_F a)^{-1} > 0$. There exists, however, also the repulsive polaron branch (solid green line) which corresponds to a higher excited state of the $\downarrow$-atom interacting repulsively with the $\uparrow$-Fermi sea. Our results for the energy of the repulsive branch agree with the weak-coupling results [18] for $(k_F a)^{-1} \gtrsim 1$. In the strong-coupling regime our energies lie between the result from the non-self-consistent T-matrix approach [21] and the MC results for square well potentials [24]. In the polaron spectral function [cf. Fig. 2(b)], one can clearly discern the attractive polaron branch as a very sharp peak at low

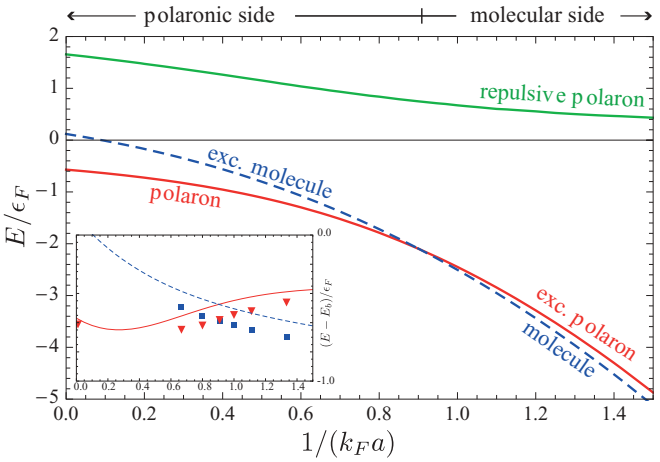

FIG. 3. (Color online) Energy spectrum of the single-particle excitations of the polaron-to-molecule transition. In the inset we show our fRG result for the ground-state energy [with the universal dimer binding energy $E_b = -\hbar^2/(ma^2)$ subtracted] in comparison to the results obtained with diagMC by Prokof'ev and Svistunov [2] (symbols).

frequencies, and the much broader repulsive polaron branch at higher frequencies.

Decay widths. The repulsive polaron has a large decay width $\Gamma_{\rm rep}$, as calculated from Eq. (23) and depicted in Fig. 5, and correspondingly a short lifetime. The leading-order decay channel for the repulsive polaron is the process shown in Fig. 4 (left) where the repulsive polaron, which is an excited state, decays to the attractive, and energetically lower lying, polaron due to the interaction with an ↑-atom. This diagram can be translated via the optical theorem into a contribution to the imaginary part of the ↓-atom self-energy, as depicted in Fig. 4 (right). This self-energy diagram is already included in the non-self-consistent T-matrix propagator $P_\downarrow^{\rm nsc}$, and has been studied recently using this approximation [21]. Of course, this diagram is also included in our fRG approach.

In the weak-coupling limit $(k_F a)^{-1} \to \infty$, the excitation becomes sharp, $\Gamma_{\rm rep} \to 0$, and the repulsive polaron is a well-defined quasiparticle. Toward unitarity, $\Gamma_{\rm rep}$ grows but remains a well-defined, finite quantity even at unitarity. We find that indeed $\Gamma_{\rm rep}$, and not the approximation $\Gamma_{\rm rep}^{\rm alt}$ from Eq. (26), is the correct halfwidth at half-height of the respective peak

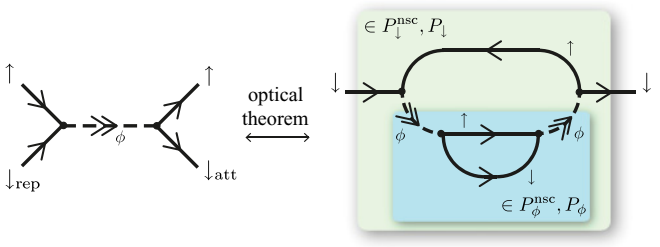

FIG. 4. (Color online) Decay channel for the repulsive polaron. (left) Two-body process which leads to the decay of the repulsive polaron. (right) Corresponding contribution to the ↓-atom self-energy via the optical theorem.

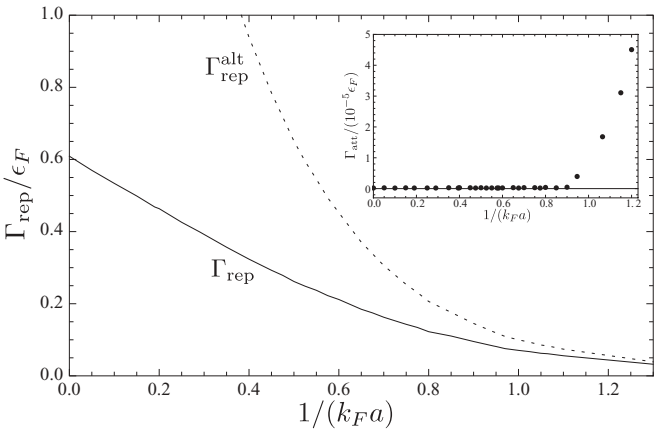

FIG. 5. Decay width $\Gamma_{\rm rep}$ of the repulsive polaron as a function of the coupling $(k_F a)^{-1}$. We also show the width according to the approximate formula Eq. (26) (dotted line). Inset: Decay width $\Gamma_{\rm att}$ of the attractive polaron.

in the polaron spectral function in Fig. 2(b). For $(k_F a)^{-1} < 0.6$ the energy $E_{\rm rep}$ of the repulsive branch exceeds the bath Fermi energy; $E_{\rm rep} > \epsilon_F$. At this point it is energetically favorable to spin-flip the impurity atom, which can be interpreted as the condition for the onset of saturated ferromagnetism [20,26]. At the same time the decay width $\Gamma_{\rm rep} > 0.2\epsilon_F$ is large, which potentially destabilizes a ferromagnetic phase [25].

On the polaronic side $(k_F a)^{-1} < (k_F a_c)^{-1}$ the attractive polaron is the stable ground state with decay width $\Gamma_{\rm att} = 0$, while on the molecular side it is an excited state with finite lifetime and decay width $\Gamma_{\rm att} > 0$, see Fig. 5 (inset). This decay is much weaker and also qualitatively different from the repulsive channel. The attractive polaron can decay by a three-body recombination process as shown in Fig. 6 (left). Via the optical theorem this process can be translated into a contribution to the ↓-atom self-energy as depicted in Fig. 6 (right), plus an additional contribution with crossed lines. This decay channel has recently been studied using an explicit three-loop calculation [17]. The resulting finite lifetime cannot be seen in the non-self-consistent T-matrix approximation, where the self-energy corrections of the ↓-atom—indicated by the

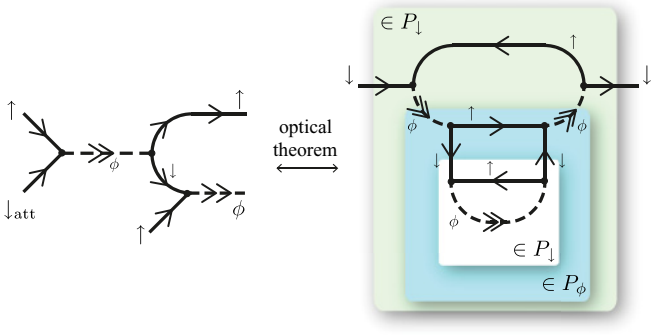

FIG. 6. (Color online) Decay channel for the attractive polaron. (left) Three-body recombination process which leads to the decay of the attractive polaron. (right) Corresponding contribution to the ↓-atom self-energy via the optical theorem (there is also a contribution with crossed lines).

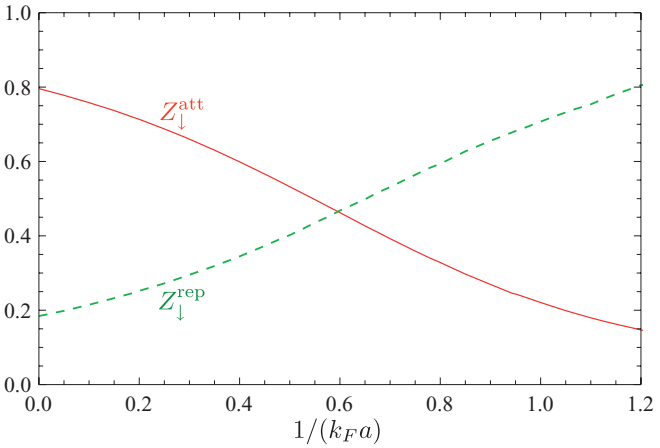

FIG. 7. (Color online) Quasiparticle weight $Z_\downarrow$ of the attractive (solid line) and repulsive (dashed line) polaron. The weights of the two quasiparticle peaks in the $\downarrow$ spectral function almost completely make up the total spectral weight, and the contribution from the incoherent background is very small.

inner white box $P_\downarrow$—are not fed back into the T-matrix $\sim P_\phi^{-1}$ [8,21]. In contrast to the non-self-consistent T-matrix calculation, our fRG includes the full feedback of both the $\downarrow$ and ϕ self-energies, denoted by bold internal lines in the flow equations in Fig. 1. Therefore, the contributions from the decay diagram in Fig. 6 (right), and many more, are automatically included in our approach.

Quasiparticle weights. Figure 7 depicts the quasiparticle weights of the attractive and repulsive polaron computed using Eq. (25). On the polaronic side the attractive polaron state contains most of the weight, but as one moves toward the molecular side the spectral weight gradually shifts to the repulsive branch, and the corresponding peak in the polaron spectral function in Fig. 2(b) becomes larger. We find that the attractive and repulsive branches almost completely make up the total spectral weight, hence the contribution from the incoherent background is very small. This is also apparent in the polaron spectral function in Fig. 2(b).

Our results for the quasiparticle weights agree well with those from the non-self-consistent T matrix and variational wave-function approaches. At unitarity we obtain for the attractive polaron $Z_{\downarrow,\rm att} = 0.796$ compared to the variational value $Z_{\downarrow,\rm att} = 0.78$ [7,10]. For the repulsive polaron at $(k_F a)^{-1} = 1$ we find $Z_{\downarrow,\rm rep} = 0.71$, in agreement with the recent non-self-consistent T-matrix calculation [21].

Note that there is an alternative definition of the quasiparticle weight [10]:

$$Z_\downarrow^{\rm alt} = \lim_{t\to\infty} |G_\downarrow(t, \mathbf{p} = 0)|. \tag{27}$$

This definition has to be treated with care. On the molecular side of the transition the polaron acquires a finite decay width $\Gamma_\downarrow > 0$ but nonetheless continues to be a well-defined quasiparticle with finite spectral weight, as can be seen from Fig. 2. However, definition (27) yields zero as soon as $\Gamma_\downarrow > 0$ and in this case cannot be interpreted as a measure of spectral weight anymore. In contrast, the definition (25) remains correct for a finite decay width and accordingly our data for $Z_\downarrow$ show no discontinuity at the transition. In the experiment the finite lifetime of the attractive polaron on the molecular side complicates the direct measurement of $Z_\downarrow$ by radiofrequency spectroscopy because the molecular state and not the attractive polaron becomes occupied as the initial state (cf. Sec. V).

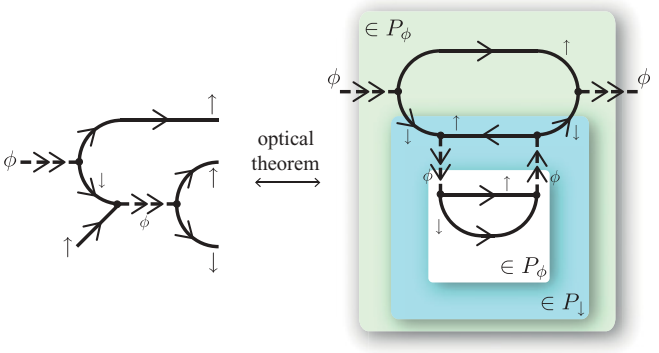

FIG. 8. (Color online) Leading decay channel for the excited molecular state. (left) Three-body recombination process which leads to the decay of the molecular state. (right) Corresponding contribution to the molecule self-energy via the optical theorem (there is also a contribution with crossed lines).

B. Molecule

Energy spectrum. The molecule spectral function in Fig. 2(d) displays a sharp quasiparticle peak of the bound state at low frequencies, followed by an incoherent background at higher frequencies which actually carries most of the spectral weight. Note that this background is not taken into account in the simple derivative expansion in the appendix nor in the Wilsonian RG approach [15]. On the molecular side $(k_F a)^{-1} > (k_F a_c)^{-1}$, the molecule is the ground state and is clearly separated from the incoherent continuum. On the polaronic side of the transition the molecule becomes an unstable, excited state and develops a clearly visible finite decay width in the spectral function.

Decay widths. The leading decay channel of the excited molecule state is via the three-body recombination process shown in Fig. 8 (left). Via the optical theorem this process can be translated into a contribution to the molecule self-energy as depicted in Fig. 8 (right). Similarly to the attractive polaron, in the non-self-consistent T-matrix approximation, the $\downarrow$-atom self-energy corrections in $P_\downarrow$ are not fed back into the T-matrix $\sim P_\phi^{-1}$, and the molecule does not decay. In contrast, the diagram Fig. 6 (right) is included in the fRG, which leads to the visible broadening in the spectral function.

Reference [17] shows by an analytical calculation of the phase space for three-loop diagrams of the type in Fig. 8 that the decay width of the molecule scales as

$$\Gamma_\phi \propto \Delta\omega^{9/2}, \quad \Delta\omega = E_\phi - E_{\downarrow,\rm att}, \tag{28}$$

where $\Delta\omega$ is the difference between the energy levels of the excited molecule and the attractive polaron ground state. In Fig. 9 we show Γ_ϕ as a function of $\Delta\omega$ in a double logarithmic plot. The large fluctuations of our numerical data are due to the accuracy of the Runge-Kutta integration as well as due to the restriction to a finite number of Matsubara frequencies.

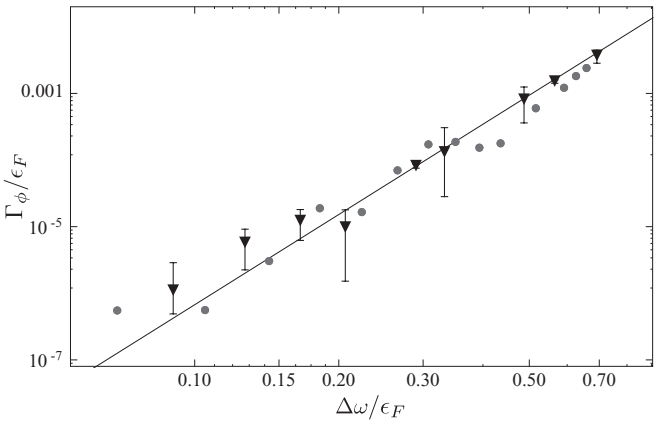

FIG. 9. The decay width Γ_ϕ of the excited molecular state as a function of the energy difference $\Delta\omega = E_\phi - E_{\downarrow,\mathrm{att}}$ between the excited molecule and the attractive polaron ground state. The solid line indicates the power-law scaling $\Gamma_\phi \propto \Delta\omega^{9/2}$.

We have estimated the corresponding error by comparing the results for different grids with varying number and position of (Matsubara) frequencies. The solid line in Fig. 9 indicates the power law $\Delta\omega^{9/2}$. The triangles in Fig. 9 correspond to a calculation with a higher number of frequencies and we find a convergence to the solid curve for decay widths larger than our numerical integration accuracy $\epsilon = 10^{-5}$. This indicates that the error for larger Γ_ϕ can be attributed to the Padé approximation, while for $\Gamma_\phi < \epsilon$ the accuracy of our results becomes limited by the absolute error of our numerical integration. With our fRG calculation we are thus able to verify the prediction by Bruun and Massignan [17], and the correctness of the power law attests to the strength of our method to describe many features of the polaron-to-molecule transition in one unified approach.

Quasiparticle weight and compositeness. The quasiparticle weight Z_ϕ of the molecular bound state in the spectral function in Fig. 2(d) is very small, $Z_\phi \approx 0.002$ at unitarity, and increases slowly toward the molecular limit, see Fig. 10 (inset). For broad resonances, $h^2 \sim \Delta B \to \infty$, the two-channel model (2) is equivalent to the single-channel model (1) where $Z_\phi = 0$ [31].

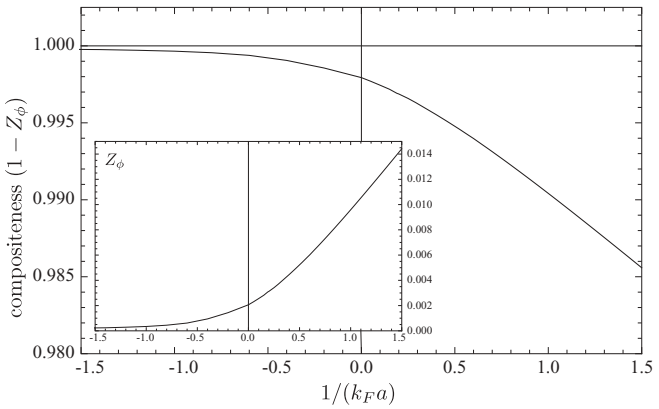

FIG. 10. Compositeness $(1 - Z_\phi)$ of the molecular bound state. A value of 100% would indicate that the molecule has no overlap with elementary closed-channel bosons. Inset: Molecular residue Z_ϕ.

Specifically, we obtain for the weight of the bound state in vacuum

$$Z_\phi = \frac{32\pi}{h^2 a} \quad (\text{vacuum}, \Lambda \to \infty). \tag{29}$$

This is consistent with the interpretation of Z_ϕ as the closed-channel admixture (cf. Eq. (28) in [5]). In our calculation we set the physical UV cutoff scale to $\Lambda = 10^3 k_F$, which is of the order of the inverse Bohr radius, and choose $h^2 < \infty$. We observe $Z_\phi \propto 1/(k_F a)$ on the BEC side and a deviation from the vacuum scaling close to unitarity, which may be due to a combination of finite density corrections and the admixture of closed-channel molecules in the microscopic action by choosing finite values of h and Λ.

Furthermore, the quasiparticle weight Z can be interpreted as the overlap between the "true" particles and the "elementary," or bare, particles in the microscopic action (2). The attractive Fermi polaron becomes elementary, $Z_{\downarrow,\mathrm{att}} \to 1$, in the BCS limit ($k_F a \to 0^-$), while in the opposite limit of $k_F a \to 0^+$ the repulsive Fermi polaron becomes elementary, $Z_{\downarrow,\mathrm{rep}} \to 1$. Near unitarity, both excitations have a sizable weight. In contrast, the molecular bound state is almost exclusively a composite particle in the whole transition region. Indeed, the deviation of the quasiparticle weight from unity, $1 - Z_\phi$, is a well-established measure of compositeness in nuclear physics [30], and in Fig. 10 we show that, for our choice of Yukawa coupling h, the compositeness of the molecule is very large (>98%). This is consistent with the measurement of a small molecular weight Z_ϕ for a balanced ^{6}Li Fermi gas close to a broad Feshbach resonance by Partridge *et al.* [42]. In experiments with a narrow Feshbach resonance the compositeness will decrease and a single-channel description becomes invalid. A strength of the fRG approach is that both situations are naturally described by tuning the values of h and $G_{\phi,\Lambda}$.

In the vacuum there exists no molecular state for negative scattering length a as can easily seen from Eq. (7), which has no bound-state pole. In the presence of a medium of $\uparrow$-fermions, however, the molecule propagator develops an excited bound-state pole also for negative scattering length a. This bound state will become the superfluid ground state if the impurity density exceeds a critical threshold [10].

V. RF RESPONSE OF THE ^{6}LI FERMI GAS

As a final application we want to connect our results for the polaronic spectral function to experimentally observable radiofrequency (rf) spectra. The attractive branch of the polaron-to-molecule transition has been studied experimentally by Schirotzek *et al.* [6] using a population imbalanced, two-component mixture of ^{6}Li atoms. In the experiment the rf response of the system has been used to infer information about the low-frequency behavior of the fermionic spectral functions. For instance, the ground-state energy and the residue $Z_\downarrow$ of the $\downarrow$-fermions were measured and confirmed the theoretical predictions.

In order to measure the rf response, an rf pulse is applied to the system which drives the transition of the atoms to a third, initially empty state. In Fig. 11 we show the scattering length profile of ^{6}Li versus the magnetic field. In the experiment [6]

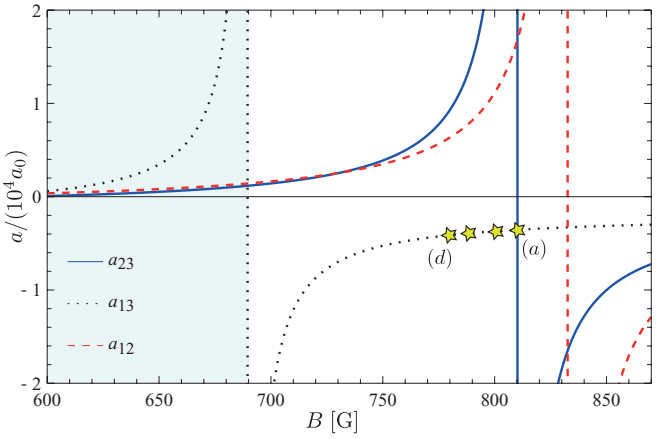

FIG. 11. (Color online) Scattering length profile of ^{6}Li atoms in the three lowest hyperfine states as calculated by P. S. Julienne based on the model described in [43]. The stars indicate the magnetic field values for which we determine the rf response of the imbalanced Fermi gas in Fig. 13.

a mixture of fermions initially in the hyperfine states $|1\rangle$ and $|3\rangle$ had been prepared in a range of the external magnetic field $B = 630 \ldots 690$ G (shaded area). In this regime the scattering length a_{13} in the initial state is large and positive, while the final-state scattering lengths a_{12} and a_{23} are rather small.

Information about the spectral function can be accessed from rf spectroscopy; for example, by populating the particle under investigation up to the energies one is interested in and then driving the transition to a weakly interacting final state for which the spectral function is well known. This route had been taken for the study of the attractive polaron. The repulsive polaron branch, on the other hand, has not yet been observed directly in experiments. The main complication is that the repulsive polaron has a very short lifetime in the strong-coupling regime of interest (cf. Fig. 5). Hence, its macroscopic population is inhibited on longer time scales, and even after a fast ramp to the desired magnetic field most minority atoms will have decayed into the respective ground state. A similar situation arises in the detection of Efimov trimers in a three-component mixture of ^{6}Li atoms [44,45]. The decay of the repulsive branch is also of relevance for the balanced system and the competition between ferromagnetic order and molecule formation [22,25].

In this section we propose an experimental procedure to circumvent these difficulties and directly analyze the spectral function of the repulsive polaron. A strongly imbalanced two-component ^{6}Li Fermi gas is prepared in hyperfine states $|1\rangle$ and $|3\rangle$ for magnetic fields $B > 690$ G across the (1,3) Feshbach resonance. In this regime the initial scattering length is negative, $a_{13} < 0$. One then drives an rf transition to the final state $|2\rangle$ which is characterized by large, positive scattering lengths a_{12} and a_{23} and thus strong interactions. Because the attractive polaron spectral function of the initial state, with its negative scattering length a_{13}, is well understood both experimentally and theoretically, the final-state spectral function can then be analyzed in a controlled fashion.

Within linear response theory the induced transition rate from the initial state $|i\rangle$ to the final state $|f\rangle$ is given by [46–48]

$$I(\omega_L) = 2\Omega^2 \,\mathrm{Im}\,\chi_R(\mu_f - \mu_i - \omega_L), \tag{30}$$

where the Rabi frequency Ω is given by the coupling strength of the rf photon to the atomic transition, μ_i (μ_f) is the initial (final) state chemical potential, and ω_L denotes the rf frequency offset with respect to the free rf transition frequency. Neglecting the momentum of the rf photon, the retarded rf susceptibility χ_R is given by the analytical continuation to real frequencies of the correlation function in imaginary time τ (Matsubara frequency ω)

$$\chi(\omega) = -\int_{\mathbf{r}}\int_{\mathbf{r}'}\int_{\tau} e^{i\omega\tau}\langle T_\tau \psi_f^\dagger(\mathbf{r},\tau)\psi_i(\mathbf{r},\tau)\psi_i^\dagger(\mathbf{r}',0)\psi_f(\mathbf{r}',0)\rangle, \tag{31}$$

where T_τ is the imaginary time-ordering operator. Eq. (31) leads to various diagrammatic contributions which are in general difficult to handle if the final-state interactions are not negligible [49]. Here we will calculate Eq. (31) in a simple approximation with full Green's functions but without vertex corrections. In this approximation Eq. (31) yields the susceptibility in Matsubara frequency:

$$\chi(\omega) = \int_{\mathbf{k},\nu} G_i(\mathbf{k},\nu)G_f(\mathbf{k},\nu+\omega). \tag{32}$$

The rf response in real frequency is then given by

$$I(\omega_L) = \Omega^2 \int_{\mathbf{k}}\int_0^{\mu_i-\mu_f+\omega_L} \frac{d\nu}{2\pi} \times A_f(\mathbf{k},\nu)\, A_i(\mathbf{k},\nu+\mu_f-\mu_i-\omega_L), \tag{33}$$

where $\mu_i - \mu_f + \omega_L > 0$.

In Eq. (33) the initial-state spectral function A_i is probed for negative frequencies only. Hence, there is no rf response for the pure polaron problem at vanishing density and chemical potential $\mu_\downarrow^{(0)}$. In the experiment one has, however, a small but finite concentration $x = n_\downarrow/n_\uparrow$ of $\downarrow$-fermions which leads to an observable rf response. In order to describe the experimental situation we therefore need a calculation for a finite minority ($\downarrow$) density characterized by a chemical potential $\mu_i = \mu_\downarrow > \mu_\downarrow^{(0)}$. Within the fRG framework such a calculation requires the regulator $R_\downarrow$ in Eq. (10) to be adjusted in order to cope with the finite Fermi surface of $\downarrow$-fermions which complicates the computation. Fortunately, our calculation for the polaron problem shows that, for negative scattering length, where the polaron is the ground state and decay processes do not matter, the fRG results are in excellent agreement with the results from a non-self-consistent T-matrix approach. We may therefore use this approach instead of a full-feedback fRG for the calculation of the imbalanced Fermi gas of finite densities $n_\uparrow$ and $n_\downarrow$ in order to determine the initial-state spectral function. The non-self-consistent calculation was also done by Punk and Zwerger [46] and is obtained in our fRG formulation by simply switching off the feedback of the $\downarrow$-atom self-energy into the molecule flow.

Because the occupation of $\downarrow$-atoms is small only the low-momentum modes are relevant. The $\downarrow$-atoms form a

degenerate Fermi gas of polaronic quasiparticles and the spectral function can be approximated by [16]

$$A_i(\omega,\mathbf{p}) = 2\pi Z_i \delta\left(\omega - \frac{\mathbf{p}^2}{2m_\downarrow^*} + \Delta\right), \tag{34}$$

where Z_i is the residue and $m_\downarrow^*$ is the effective mass of the impurity atoms. Δ determines the impurity concentration x.

We have calculated the parameters $m_\downarrow^*$, Z_i, and Δ as functions of $(k_F a)^{-1}$ via the non-feedback (non-self-consistent T-matrix) calculation. μ_i is determined self-consistently to ensure the correct impurity density. Inserting the spectral function Eq. (34) into the susceptibility (33) we obtain for the rf response

$$I(\omega_L) = \frac{\Omega^2 Z_i}{2\pi^2}\int_0^{\sqrt{2m_\downarrow^*\Delta}} d k \mathbf{k}^2 \times A_f\left(\mathbf{k}, \mu_i - \mu_f + \omega_L - \Delta + \frac{\mathbf{k}^2}{2m_\downarrow^*}\right). \tag{35}$$

For the final state $|f\rangle$ we use the spectral function obtained in Sec. IV from the full fRG calculation. In Fig. 12 we show an example of the full final-state spectral function dependent on frequency and momentum which enters the momentum sum in Eq. (35). One can clearly discern the broadening of the attractive polaron branch at larger momenta, as well as the broad repulsive branch at higher frequencies. A similar feature appears in the spectral function for the balanced Fermi gas above T_c as calculated by Haussmann *et al.* [48]. The fermionic spectral functions and rf spectra in this work were determined using state-of-the-art self-consistent T-matrix (2PI) approximations and form the basis for a full linear response calculation including vertex corrections [50].

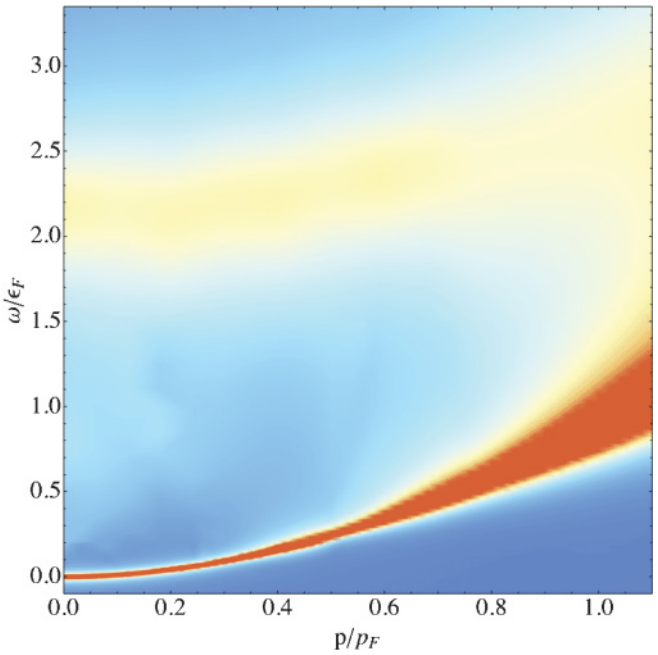

FIG. 12. (Color online) Full momentum and frequency dependence of the polaron spectral function $A_\downarrow(\omega,\mathbf{p})$ at unitarity $(k_F a)^{-1} = 0$.

TABLE II. Interaction parameters at the four transitions indicated in Fig. 11, using $k_{F\uparrow} = 0.000\,15 a_0^{-1}$.

	B field [G]	$(k_F a_{13})^{-1}$	$(k_F a_{23})^{-1}$	$(k_F a_{12})^{-1}$
(a)	810.3	−1.88	0.0	0.39
(b)	800.8	−1.80	0.2	0.58
(c)	788.2	−1.70	0.5	0.86
(d)	780.6	−1.62	0.7	1.04

Initially, the gas is prepared in a $|1\rangle$ and $|3\rangle$ mixture, and both states can serve as minority or majority species; for example, $|\uparrow\rangle = |3\rangle$ and $|\downarrow\rangle = |1\rangle$ such that $|i\rangle = |1\rangle$ and $|f\rangle = |2\rangle$. The initial occupation of the minority $|\downarrow\rangle$ states is small and, for our numerical calculation, we use $x = n_\downarrow/n_\uparrow = 0.01$. The energy scale is set by the Fermi momentum of the majority species $k_{F\uparrow} = 0.000\,15 a_0^{-1}$ as appropriate for the experiment in Ref. [6]. We calculate the rf spectra at the four values of the magnetic field indicated as stars in Fig. 11, and listed in Table II. The resulting spectra are shown in Fig. 13: the solid blue lines indicate the response for minority species $|1\rangle$, while the dashed red lines correspond to minority species $|3\rangle$. In the latter case the sign of the frequency offset ω_L is changed because the state $|3\rangle$ is energetically above the final state.

The position of the sharp attractive polaron peak at negative frequency offset ω_L shifts with the interaction parameter

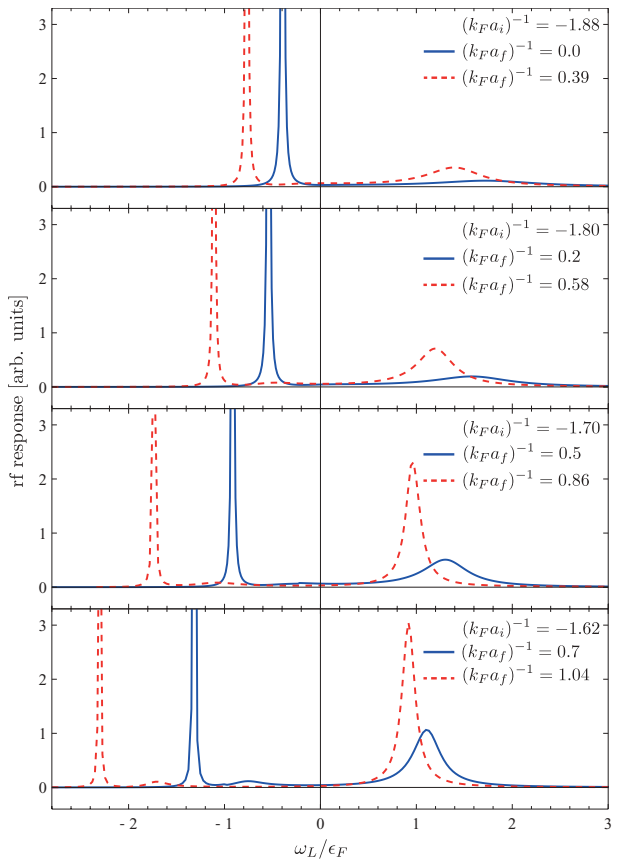

FIG. 13. (Color online) rf spectra $I(\omega_L)$ for minority species $|1\rangle$ (solid blue lines) and minority species $|3\rangle$ (dashed red lines). The interaction parameters correspond to the four magnetic field values marked in Fig. 11, and listed in Table II: (a) top–(d) bottom.

$(k_F a_f)^{-1}$ in accordance with the energy spectrum Fig. 3. One observes that the attractive polaron loses quasiparticle weight on the molecular side (cf. Fig. 7). In contrast, the repulsive polaron branch gains quasiparticle weight toward the molecular side, and the respective peak in the rf spectra becomes both larger and narrower, and one can read of the increasing lifetime.

The spectra in Fig. 13 are convolved with the sinc function $\mathrm{sinc}^2(\omega T/2)$, which gives the response to an rf pulse with a rectangular profile of length $T = 20$ ms [48]. While our curves are computed for zero temperature, a finite temperature $\sim 0.01 T_F$ would lead only to a slight broadening of the experimental rf peaks. The broadening of the attractive polaron due to the finite lifetime on the molecular side $(k_F a_f)^{-1} > (k_F a_c)^{-1}$, however, is too small to be resolved. Note that we have included both final-state and initial-state interactions in our calculation: the knowledge of the spectral function for the initial state allows for a detailed study of the final-state spectral function.

VI. DISCUSSION

We have developed and presented a computational method to solve the nonperturbative, exact renormalization group equation (3) and have demonstrated its efficiency for the Fermi polaron problem as a specific example. The inclusion of the full frequency and momentum dependence of the propagators opens up new perspectives to apply the functional renormalization group to problems where the detailed dynamics of the relevant degrees of freedom becomes important [51]. In particular, the method draws its strength from the possibility to successively bosonize further channels of the interaction via additional auxiliary fields (Hubbard-Stratonovich transformation) [52]. In this way one can partially capture the complicated analytical structure of higher-order vertex functions $\Gamma^{(n)}$, including possible quasiparticle poles and branch cuts, as we have explicitly shown for the s-wave scattering channel in the polaron problem. In combination with the recently developed flowing rebosonization technique [41] our numerical method can be extended to also incorporate re-emerging vertices. Our approach complements the proposal for bosons [29] and additionally includes fermions.

For the Fermi polaron problem we achieve a unified description of many dynamical effects beyond thermodynamics. We verify the nontrivial power-law scaling of decay rates [17] and determine the properties of the repulsive polaron with a method beyond the non-self-consistent T-matrix approximation [20,21]. This is of value in the ongoing debate about the possible occurrence of ferromagnetism in ultracold Fermi gases with short-range interactions [20–26]. The polaron problem sheds light on this question in the limit of strong population imbalance. For the repulsive polaron we find the critical interactions strength $k_F a = 1.57$ from our numerical data (Fig. 3). Going to a finite density of $\downarrow$-fermions is straightforward within the fRG and involves only a slight modification of the regulator of the $\downarrow$-fermions (10) as long as no spontaneous symmetry breaking occurs. By continuity we can infer that the repulsive branch will remain to exist for small but finite $\downarrow$-population and will exceed the critical energy ϵ_F for the presumed onset of saturated ferromagnetism. It is an open question whether, for larger impurity concentrations, the repulsive branch is so strongly renormalized that saturated ferromagnetism can be ruled out [26], or whether competition with molecule formation may preclude the observation of ferromagnetic domains [25]. Answering these questions will require a full nonequilibrium calculation.

There has been much theoretical progress on the repulsive Fermi gas with short-range interactions, but relatively few experiments have been completed. While the repulsive ^{3}He Fermi gas has been studied extensively in experiment, it is not dilute and has a large repulsive hard-core potential [53]. In contrast, ultracold Fermi gases offer the realization of a proper contact interaction of tunable strength. We predict rf transition rates for the repulsive branch and propose a possible route to measure these excited states in a ^{6}Li Fermi gas. This is a challenging problem because the final repulsive polaron state is highly unstable. One possible approach could involve fast tomographic imaging similar to the MIT experiment [6], another might be to measure the loss in the final state which is expected to scale with the rf transition rate for a constant rf pulse time but may be suppressed by the quantum Zeno effect [44]. Hence, the possible observation of the repulsive polaron represents not only a test of theoretical predictions but poses an interesting challenge touching several aspects of many-body physics.

ACKNOWLEDGMENTS

We wish to thank M. Barth, N. Dupuis, T. Hyodo, S. Jochim, N. Kaiser, S. Moroz, M. Punk, S. Rath, and W. Zwerger for many useful discussions and P. Julienne, N. Prokof'ev, B. Svistunov, and M. Zwierlein for kindly providing their data for comparison. Part of this work was supported by the DFG within the Forschergruppe 801.

APPENDIX: DERIVATIVE EXPANSION

In this appendix we qualitatively study the polaron-to-molecule transition using a simple approximation for the renormalized Green's functions $G_{\downarrow,k}$ and $G_{\phi,k}$. As we have seen, $G_{\downarrow,k}$ and $G_{\phi,k}$ generally develop a complicated frequency and momentum $(\omega,\mathbf{p})$ dependence. Here, we will use an expansion in small frequencies and momenta (derivative or gradient expansion) which allows for an analytical evaluation of the loop integrals on the right-hand side of the flow equation (8). The derivative expansion proves to be a good approximation if one is interested in the physics determined by the structure of the Green's functions close to their poles, such as, for example, in the description of phase transitions and critical phenomena [32]. In the derivative expansion the dependence of the inverse propagators $P_{\downarrow/\phi,k}(\omega,\mathbf{p})$ on the RG scale k is approximated by

$$\begin{aligned} P_{\downarrow,k}(\omega,\mathbf{p}) &= A_{\downarrow,k}(-i\omega + \mathbf{p}^2) + m^2_{\downarrow,k}, \\ P_{\phi,k}(\omega,\mathbf{p}) &= A_{\phi,k}(-i\omega + \mathbf{p}^2/2) + m^2_{\phi,k}. \end{aligned} \tag{A1}$$

In this approximation, which is similar to the one used in the Wilsonian RG approach to the polaron problem [15], we assume that the renormalization of the frequency and momentum coefficients is given by common wave-function renormalizations $A_{\downarrow,k}$ and $A_{\phi,k}$, respectively, which in turn

are related to the quasiparticle weights via $Z_{\downarrow/\phi} = A^{-1}_{\downarrow/\phi}$. The flowing gap terms $m^2_{\downarrow,k}$ and $m^2_{\phi,k}$ are related to the flowing static self-energy via Eq. (11).

From equation (8) one can derive the flow equations for the four running couplings $A_{\downarrow,k}$, $A_{\phi,k}$, $m^2_{\downarrow,k}$, and $m^2_{\phi,k}$. The $\uparrow$-fermions are not renormalized; $A_{\uparrow,k} = 1$ and $m^2_{\uparrow,k} = -\mu_\uparrow$. With the sharp cutoff (10), the frequency as well as the momentum integrations can be performed analytically. The resulting flow equations read

$$\begin{aligned}
\partial_k A_\downarrow &= -\frac{2h^2k}{\pi^2 A_\phi}\theta(\mu_\uparrow - 2k^2)\left[\frac{\sqrt{\mu_\uparrow - k^2}}{\left(k^2 + \mu_\uparrow + 2m^2_\phi/A_\phi\right)^2}\right.\\
&\quad\left.+\frac{k}{\left(-k^2 + 2\mu_\uparrow + 2m^2_\phi/A_\phi\right)^2}\right],\\
\partial_k m^2_\downarrow &= \frac{h^2k}{\pi^2 A_\phi}\theta(\mu_\uparrow - 2k^2)\left[\frac{\sqrt{\mu_\uparrow - k^2}}{k^2 + \mu_\uparrow + 2m^2_\phi/A_\phi}\right.\\
&\quad\left.+\frac{k}{-k^2 + 2\mu_\uparrow + 2m^2_\phi/A_\phi}\right],\\
\partial_k A_\phi &= -\frac{h^2k}{2\pi^2 A_\downarrow}\frac{\sqrt{\mu_\uparrow + k^2}}{(2k^2 + \mu_\uparrow + m^2_\downarrow/A_\downarrow)^2},\\
\partial_k m^2_\phi &= \frac{h^2k}{2\pi^2 A_\downarrow}\frac{\sqrt{\mu_\uparrow + k^2}}{(2k^2 + \mu_\uparrow + m^2_\downarrow/A_\downarrow)}.
\end{aligned} \tag{A2}$$

The initial conditions for this system of differential equations (A2) are specified at the UV scale $k = \Lambda$. We note that the derivative expansion (A1) of the molecule propagator $P_{\phi,k}(\omega,\mathbf{p})$ cannot account for the correct vacuum scattering amplitude (5), because the term iq is rooted in the nonanalytical structure of the molecule propagator (7). We therefore focus only on the correct calculation of the scattering length a for $q = 0$, which leads to the infrared condition $(m^{\rm vac}_{\phi,k=0})^2 = -h^2/(8\pi a)$ for $\mu_\downarrow = \mu_\uparrow = 0$. In this case of two-body physics $P_{\downarrow,k}$ is not renormalized, $A_{\downarrow,k} = 1$ and $m^2_{\downarrow,k} = 0$, and the differential equations for $A_{\phi,k}$ and $m^2_{\phi,k}$ decouple and can be solved analytically. The integration of (A2) in the vacuum limit yields

$$\left(m^{\rm vac}_{\phi,k=0}\right)^2 = m^2_{\phi,\Lambda} - \frac{h^2\Lambda}{4\pi^2}. \tag{A3}$$

This leads to the UV condition for the molecule gap,

$$m^2_{\phi,\Lambda} = \frac{h^2}{8\pi}(2\Lambda/\pi - a^{-1}), \tag{A4}$$

which incorporates the correct regularization of the UV divergence Λ in Eq. (A3). At the UV scale the momentum and frequency dependence of $P_{\phi,\Lambda}$ can be neglected due to the large bosonic gap $m^2_{\phi,\Lambda}$, and we set $A_{\phi,\Lambda} = 1$.

For a finite density of $\uparrow$-atoms the system of differential equations (A2) is solved numerically. The initial values for the $\downarrow$ propagator are then given by $m^2_{\downarrow,\Lambda} = -\mu_\downarrow$ and $A_{\downarrow,\Lambda} = 1$. The down chemical potential $\mu_\downarrow$ is determined in the way discussed in Sec. II. We find that the polaron is indeed the ground state for interaction strengths $(k_F a)^{-1} < (k_F a_c)^{-1}$ whereas the molecule becomes the ground state for $(k_F a)^{-1} > (k_F a_c)^{-1}$, with $(k_F a_c)^{-1} = 0.96$.

The energy spectrum from the simple derivative expansion is in qualitative agreement and even in rough quantitative agreement with the results obtained from our new numerical method and other theoretical calculations. A drawback of the derivative expansion is that it is impossible to extract a reasonable spectral function from an ansatz of the form (A1) as it only accounts for a single coherent quasiparticle excitation. Neither higher-excited states, such as the repulsive polaron, nor the incoherent background, which comprises the major weight for the molecule (cf. Sec. IV), can be captured with this ansatz. Furthermore, although decay processes lead to a finite lifetime of the excited polaron and molecule branches, in the simple approximation (A1) these states have a vanishing decay width. Note that the finite lifetime of excited states can be obtained neither from simple variational wave functions [7] nor from the non-self-consistent T-matrix approach [8]. Their description requires the full self-energy feedback developed in Sec. III.

[1] L. D. Landau, Phys. Z. Sowjetunion **3**, 644 (1933).
[2] N. V. Prokof'ev and B. V. Svistunov, Phys. Rev. B **77**, 020408 (2008); **77**, 125101 (2008).
[3] A. C. Hewson, *The Kondo Problem to Heavy Fermions* (Cambridge University Press, Cambridge, 1997).
[4] A. Rosch and T. Kopp, Phys. Rev. Lett. **75**, 1988 (1995).
[5] I. Bloch, J. Dalibard, and W. Zwerger, Rev. Mod. Phys. **80**, 885 (2008).
[6] A. Schirotzek, C.-H. Wu, A. Sommer, and M. W. Zwierlein, Phys. Rev. Lett. **102**, 230402 (2009).
[7] F. Chevy, Phys. Rev. A **74**, 063628 (2006).
[8] R. Combescot, A. Recati, C. Lobo, and F. Chevy, Phys. Rev. Lett. **98**, 180402 (2007).
[9] R. Combescot and S. Giraud, Phys. Rev. Lett. **101**, 050404 (2008).
[10] M. Punk, P. T. Dumitrescu, and W. Zwerger, Phys. Rev. A **80**, 053605 (2009).
[11] C. Mora and F. Chevy, Phys. Rev. A **80**, 033607 (2009).
[12] R. Combescot, S. Giraud, and X. Leyronas, Europhys. Lett. **88**, 60007 (2009).
[13] M. Ku, J. Braun, and A. Schwenk, Phys. Rev. Lett. **102**, 255301 (2009).
[14] P. Nikolić and S. Sachdev, Phys. Rev. A **75**, 033608 (2007).
[15] K. B. Gubbels and H. T. C. Stoof, Phys. Rev. Lett. **100**, 140407 (2008).
[16] C. Lobo, A. Recati, S. Giorgini, and S. Stringari, Phys. Rev. Lett. **97**, 200403 (2006).
[17] G. M. Bruun and P. Massignan, Phys. Rev. Lett. **105**, 020403 (2010).
[18] R. F. Bishop, Ann. Phys. (NY) **78**, 391 (1973).
[19] T. D. Lee and C. N. Yang, Phys. Rev. **105**, 1119 (1957); K. Huang and C. Yang, *ibid.* **105**, 767 (1957).
[20] X. Cui and H. Zhai, Phys. Rev. A **81**, 041602 (2010).

[21] P. Massignan and G. M. Bruun, e-print arXiv:1102.0121.
[22] G. B. Jo, Y. R. Lee, J. H. Choi, C. A. Christensen, T. H. Kim, J. H. Thywissen, D. E. Pritchard, and W. Ketterle, Science **325**, 1521 (2009).
[23] G. J. Conduit, A. G. Green, and B. D. Simons, Phys. Rev. Lett. **103**, 207201 (2009); G. J. Conduit and E. Altman, Phys. Rev. A **83**, 043618 (2011); G. J. Conduit and B. D. Simons, *ibid.* **79**, 053606 (2009); A. Recati and S. Stringari, Phys. Rev. Lett. **106**, 080402 (2011); S. Zhang and T.-L. Ho, e-print arXiv:1102.5687.
[24] S. Pilati, G. Bertaina, S. Giorgini, and M. Troyer, Phys. Rev. Lett. **105**, 030405 (2010).
[25] D. Pekker, M. Babadi, R. Sensarma, N. Zinner, L. Pollet, M. W. Zwierlein, and E. Demler, Phys. Rev. Lett. **106**, 050402 (2011).
[26] M. Barth and W. Zwerger, Ann. Phys. (NY) in press, e-print arXiv:1101.5594.
[27] A. Bulgac and M. McNeil Forbes, Phys. Rev. A **75**, 031605 (2007).
[28] C. Wetterich, Phys. Lett. B **301**, 90 (1993).
[29] J. P. Blaizot, R. Méndez-Galain, and N. Wschebor, Phys. Lett. B **632**, 571 (2006).
[30] S. Weinberg, Phys. Rev. **137**, B672 (1965).
[31] D. Lurié and A. J. Macfarlane, Phys. Rev. **136**, B816 (1964).
[32] J. Berges, N. Tetradis, and C. Wetterich, Phys. Rep. **363**, 223 (2002).
[33] M. Salmhofer and C. Honerkamp, Prog. Theor. Phys. **105**, 1 (2001); W. Metzner, Prog. Theor. Phys. Suppl. **160**, 58 (2005); B. Delamotte, e-print arXiv:cond-mat/0702365; O. J. Rosten, e-print arXiv:1003.1366.
[34] J. Pawlowski, Ann. Phys. (NY) **322**, 2831 (2007).
[35] M. C. Birse, B. Krippa, J. A. McGovern, and N. R. Walet, Phys. Lett. B **605**, 287 (2005); S. Diehl, H. Gies, J. M. Pawlowski, and C. Wetterich, Phys. Rev. A **76**, 021602 (2007); **76**, 053627 (2007); L. Bartosch, P. Kopietz, and A. Ferraz, Phys. Rev. B **80**, 104514 (2009).
[36] S. Floerchinger, M. Scherer, S. Diehl, and C. Wetterich, Phys. Rev. B **78**, 174528 (2008).
[37] S. Diehl, H. C. Krahl, and M. Scherer, Phys. Rev. C **78**, 034001 (2008).
[38] S. Liao, J. Polonyi, and M. Strickland, Nucl. Phys. B **567**, 493 (2000); D. F. Litim, Phys. Lett. B **486**, 92 (2000).
[39] A. A. Abrikosov, L. P. Gorkov, and I. E. Dzyaloshinski, *Methods of Quantum Field Theory in Statistical Physics* (Dover, 1975).
[40] A. A. Katanin, Phys. Rev. B **70**, 115109 (2004).
[41] H. Gies and C. Wetterich, Phys. Rev. D **65**, 065001 (2002); S. Floerchinger and C. Wetterich, Phys. Lett. B **680**, 371 (2009); S. Floerchinger, Eur. Phys. J. C **69**, 119 (2010).
[42] G. B. Partridge, K. E. Strecker, R. I. Kamar, M. W. Jack, and R. G. Hulet, Phys. Rev. Lett. **95**, 020404 (2005).
[43] M. Bartenstein *et al.*, Phys. Rev. Lett. **94**, 103201 (2005).
[44] T. Lompe, T. B. Ottenstein, F. Serwane, A. N. Wenz, G. Zürn, and S. Jochim, Science **330**, 940 (2010).
[45] S. Nakajima, M. Horikoshi, T. Mukaiyama, P. Naidon, and M. Ueda, Phys. Rev. Lett. **106**, 143201 (2011).
[46] M. Punk and W. Zwerger, Phys. Rev. Lett. **99**, 170404 (2007).
[47] M. Punk, Ph.D. thesis, Technical University Munich (2009).
[48] R. Haussmann, M. Punk, and W. Zwerger, Phys. Rev. A **80**, 063612 (2009).
[49] P. Pieri, A. Perali, and G. C. Strinati, Nature Phys. **5**, 736 (2009).
[50] T. Enss, R. Haussmann, and W. Zwerger, Ann. Phys. (NY) **326**, 770 (2011).
[51] C. Honerkamp, H. C. Fu, and D. H. Lee, Phys. Rev. B **75**, 014503 (2007).
[52] C. Husemann and M. Salmhofer, Phys. Rev. B **79**, 195125 (2009).
[53] P. Wölfle and D. Vollhardt, *The Superfluid Phases of Helium 3* (Taylor and Francis, 1990).